Progress In Electromagnetics Research, Vol. 172, 13–22, 2021

Tunable Topological Refractions in Valley Sonic Crystals with Triple Valley Hall Phase Transitions

Ding Jia[1], Yin Wang[1], Yong Ge[1], Shou-Qi Yuan[1], and Hong-Xiang Sun[1, 2, *]

(*Invited Paper*)

Abstract—Topological refractions created by valley sonic crystals (VSCs) have attracted great attentions in the communities of physics and engineering owing to the advantage of zero reflection of sound and the potential for designing advanced acoustic devices. In previous works, topological refractions of valley edge states are demonstrated to be determined by the projections of the valleys K and K′, and two types of topological refractions generally exist at opposite terminals or different frequency bands. However, the realization of tunable topological refractions at the fixed frequency band and terminal still poses great challenge. To overcome this, we report the realization of tunable topological refractions by VSCs with triple valley Hall phase transitions. By simply rotating rods, we realize 3 types of topological waveguides (T1, T2, and T3) composed of two VSCs, in which the projections of the observed valley edge states can be modulated between K and K′. Additionally, based on the measured transmittance spectra, we experimentally demonstrate that these valley edge states are almost immune to backscattering against sharp bends. More importantly, we realize tunable topological refractions at the fixed frequency band and terminal, and experimentally observe the coexistence of positive and negative refractions for T1 and T3, and negative refractions for T2. The proposed tunable topological refractions have potential applications in designing multi-functional sound antennas and advanced communication devices.

1. INTRODUCTION

Recently, the research on valley degree of freedom has become a hot topic due to its potential as an excellent candidate of information carrier and important applications in information communication and processing [1–6]. Inspired by the valleytronics, researchers have introduced this concept into several subfields of physics, such as photonics [7–19], mechanics [20–26], and acoustics [27–41]. In acoustics, by breaking mirror [28–31, 35, 38–40] or inversion [33, 36, 37] symmetry, various types of valley topological transports with negligible inter-valley scatterings have been demonstrated by designing a pair of valley sonic crystals (VSCs) with opposite valley Hall phases. With these advantages, the valley topological transports have shown the potential applications in designing valley-selective acoustic emitters [28], valley-chirality locked beam splitters [27], sound delay lines [31], directional acoustic antennas [30], and acoustic concentrators [38].

In addition to the valley topological transports, reflection-free topological refractions [30, 36, 39, 42, 43] created by valley sonic crystals (VSCs) have also attracted great attentions, which can effectively solve a difficult problem of impedance mismatch at a terminal between a domain wall composed of two VSCs and an external space and design advanced topological devices of sound. Based

Received 20 October 2021, Accepted 16 December 2021, Scheduled 20 December 2021

* Corresponding author: Hong-Xiang Sun (jsdxshx@ujs.edu.cn).

[1] Research Center of Fluid Machinery Engineering and Technology, School of Physics and Electronic Engineering, School of Computer Science and Communications Engineering, Jiangsu University, Zhenjiang 212013, China. [2] State Key Laboratory of Acoustics, Institute of Acoustics, Chinese Academy of Sciences, Beijing 100190, China.

on the momentum conservation theory, topological refractions of sound can be evaluated quantitatively [30], and the refraction directions of valley edge states are experimentally demonstrated to be determined by the projections of the valleys K and K′ [28]. Generally, at the same frequency band, two distinct topological refractions can be observed at the opposite terminals of the domain wall, which arise from the fact that the edge states propagating from both sides are projected from the valleys K and K′ separately [28]. Meanwhile, by introducing a type of dual-band VSC, at two different frequency bands, the valleys K and K′ can be locked to the same propagation direction of the domain wall, and therefore, two types of topological refractions can be obtained at the same terminal [39]. However, there is still great challenge to realize tunable topological refractions at the fixed frequency band and terminal, which is very important for developing multi-functional topological devices of sound.

In this work, we here experimentally study tunable topological refractions created by VSCs composed of windmill-like rods (WMRs). By simply rotating the WMRs, we can realize a triple valley Hall phase transition in the VSCs and design 3 types of topological waveguides (T1, T2, and T3) composed of two VSCs with different rotation angles of WMRs. The observed edge states support valley topological transports and are almost immune to backscattering against sharp bends, which is experimentally demonstrated by the measured transmittance spectra of valley edge states. More importantly, based on the experimental mapping of the out-coupling of the valley edge states into the ambient space, we realize the modulation of topological refractions at the fixed frequency band and terminal, which arises from the fact that the projections of the observed valley edge states can be directly converted between K and K′ by simply rotating the WMRs. The theoretical, numerical, and experimental results agree well with each other. The proposed VSCs pave a way to design advanced topological devices with multiple functions.

2. RESULTS AND DISCUSSIONS

As schematically shown in Figure 1(a), we propose an airborne triangular-lattice SC consisting of WMRs (with a lattice constant $a = 30\,\mathrm{mm}$), in which the WMRs are fabricated with polymethyl methacrylate (PMMA) by laser cutting process technique. The parameters of the WMR are selected as $l_1 = 12.5\,\mathrm{mm}$, $l_2 = 5.0\,\mathrm{mm}$, $h_1 = 5.0\,\mathrm{mm}$, and $h_2 = 5.0\,\mathrm{mm}$, and its rotation angle θ can be modulated to realize different valley states. Throughout this work, the COMSOL Multiphysics software based on the finite element method is introduced to simulate sound propagations. In the numerical models, the module of Acoustic-Solid interaction is adopted, and the size of mesh element is smaller than $\lambda/10$ to ensure computing precision. The material parameters in the numerical model are as follows: the density $\rho = 1180\,\mathrm{kg/m^3}$, the longitudinal wave velocity $c_l = 2730\,\mathrm{m/s}$, and the transversal wave velocity $c_t = 1430\,\mathrm{m/s}$ for PMMA; $\rho_0 = 1.21\,\mathrm{kg/m^3}$ and $c_0 = 340\,\mathrm{m/s}$ for air.

Figure 1(b) shows the eigenfrequencies of band edges at the valley K of the SCs with different values of θ. It is observed that, in the range 0°–60°, three Dirac cones I, II, and III exist simultaneously, which correspond to $\theta = 8.28°$, 28.16°, and 52.14°, respectively. Here, the acoustic valley Hall (AVH) phases can be featured by the signs of the effective mass [28] $\mathrm{sgn}(m) = \mathrm{sgn}(\omega_{q+} - \omega_{p-})$, in which ω is the eigenfrequency of the valley edge state, and the subscripts q^+ and p^- are the anticlockwise and clockwise vortex pseudospins of energy flux around the points q and p, respectively. Note that the sign of m changes 3 times from $\theta = 0°$ to 60°. Therefore, without changing the structure of the WMRs, we can realize triple AVH phase transitions by simply rotating the WMRs. To demonstrate it, we simulate the dispersion relations of 3 SCs composed of the WMRs with $\theta = 8.28°$, 28.16° and 52.14°, which are shown in Figures 1(c)–1(e), respectively. We can see that there exists a Dirac cone for three cases, and the eigenfrequencies of these Dirac cones are almost the same. Therefore, by simply adjusting the rotation angle θ of the WMRs, we can realize triple AVH phase transitions in the same band, which provides the feasibility for realizing tunable topological refractions of sound.

Next, we select 6 SCs with different values of θ to design a tunable valley topological material, in which the selected 6 rotation angles are distributed on both sides of the 3 Dirac cones. Figures 2(a)–2(f) show the simulated dispersion relations of the 6 SCs which correspond to the rotation angles of 0°, 11°, 25°, 32°, 44°, and 58°, respectively. The pressure amplitude eigenfunctions for K1–K12 are displayed in the middle region, in which black arrows represent the direction of energy flux. As shown in Figures 2(a) and 2(b), by changing the rotation angle θ, the coupling strength between the WMRs

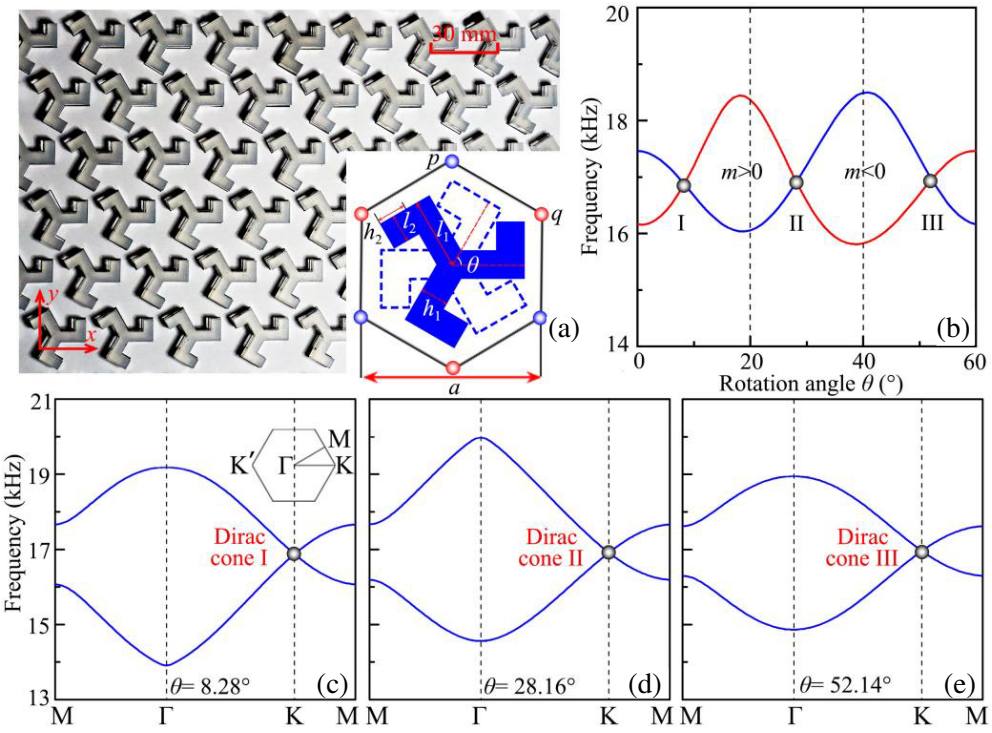

Figure 1. (a) Photograph of a triangular-lattice SC composed of WMRs. Blue solid and dashed lines in the lower-right corner represent the original configuration ($\theta = 0°$) of the WMR and its rotation state with the rotation angle of θ, respectively. Blue and red points are two inequivalent triangular-lattice centers. (b) Eigenfrequencies of band edges at the valley K with different values of θ. Dispersion relations of the SCs composed of the WMRs with (c) $\theta = 8.28°$, (d) 28.16° and (e) 52.14°, corresponding to the Dirac cones I, II and III, respectively. Inset in (c) represents the 1st Brillouin zone, in which K and K′ are two inequivalent valleys in the momentum space.

increases gradually, which destroys the two-fold degeneracy and opens the band gap of the SC-A ($\theta = 0°$) and SC-B ($\theta = 11°$), and meanwhile, the bands are inversed between the two SCs. Additionally, the sound vortexes are centered at the phase singular point q (red circular arrows) for K1 and K4, and the point p (blue circular arrows) for K2 and K3, showing typical characteristics of the band inversion and AVH phase transition between the two SCs.

Furthermore, we also find the phenomena of the band inversion between the SC-C and SC-D and between the SC-E and SC-F [shown in Figures 2(c)–2(f)]. More interestingly, the chirality of the valley vortexes for K1(K2) and K3(K4) is opposite to that for K5(K6) and K7(K8), but is the same as that for K9(K10) and K11(K12), so are the features of the triple AVH phase transitions around the 3 Dirac cones.

By simply rotating the WMRs, we design 3 types of topological waveguides composed of two VSCs, in which the waveguides T1–T3 correspond to the SC-A and SC-B, the SC-C and SC-D, and the SC-E and SC-F, respectively. Figures 3(a)–3(c) show the structures of T1–T3, in which red dashed lines and black dashed rectangles represent the domain walls and supercells, respectively, and the simulated dispersion relations for T1–T3 are displayed in Figures 3(d)–3(f), respectively. As shown in Figure 3(d), there exists a pair of edge states (red solid lines) inside the overlapped bulk bandgap of the SC-A and SC-B [shown in Figures 2(a) and 2(b)], which are located at the domain wall of T1. Here, it is noted that the group velocity of the edge states is determined by the slope of two bands in the bulk bandgap. As an example, the group velocity of the edge state φ_R^+ (corresponding to the projection of the valley K) is positive. This is because the valley Chern numbers of the first band for the SC-A and SC-B around the valley K are $1/2$ and $-1/2$, respectively, which are obtained by numerical integration of the Berry curvatures shown in the Supporting Information. Therefore, the variation of the valley Chern number

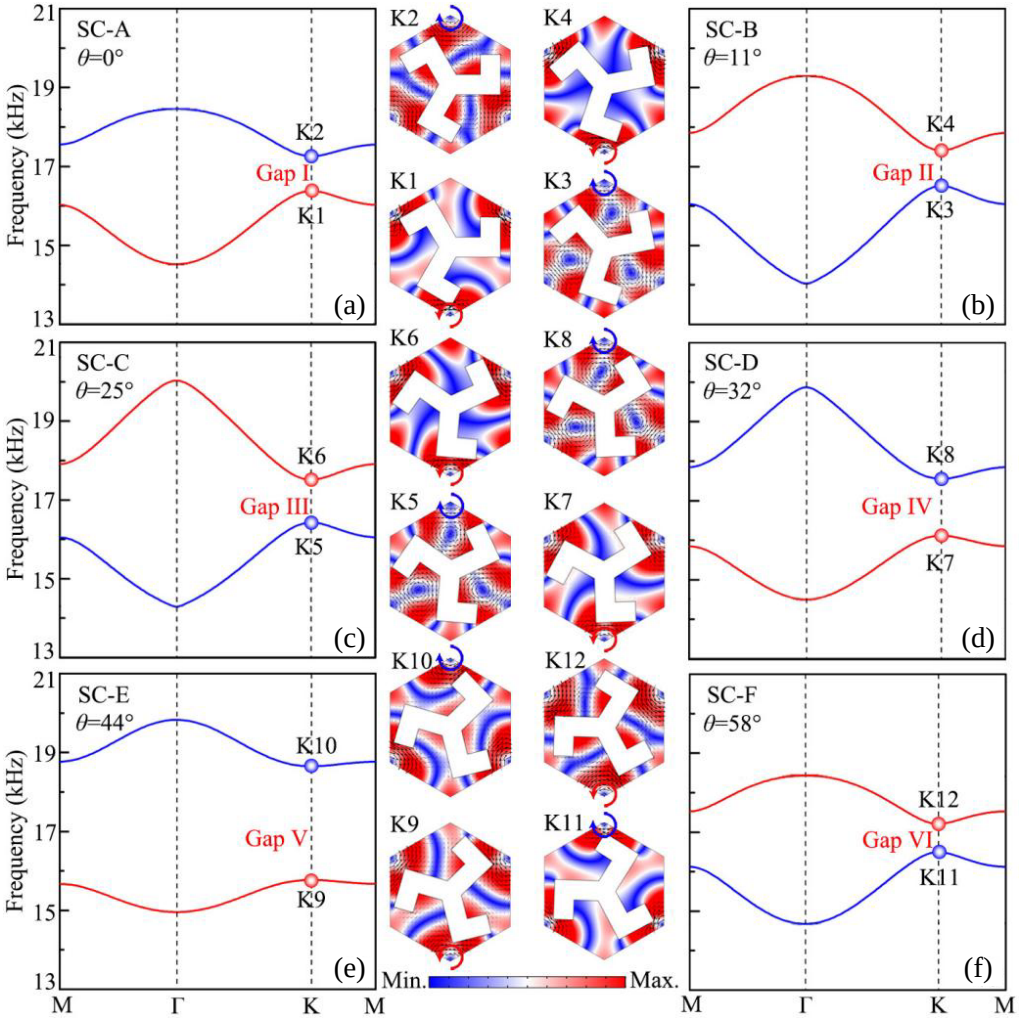

Figure 2. Simulated dispersion relations of 6 SCs composed of the WMRs with (a) $\theta = 0°$, (b) 11°, (c) 25°, (d) 32°, (e) 44° and (f) 58°. Simulated pressure amplitude eigenfunctions for K1–K12 are in the middle region. Blue and red circular arrows are the directions of energy flux surrounding the points p and q, respectively.

$\Delta C_K = C_K(\text{SC-A}) - C_K(\text{SC-B}) = 1$, which guarantees the existence of the topological edge state at the domain wall of T1. On the contrary, the group velocity of the edge state φ_L^+ (corresponding to the projection of the valley K′) is negative, which arises from an opposite valley Chern number around the valley K′ (see the Supporting Information). Moreover, a pair of edge states can also be observed in T2 and T3. Compared with the results in Figure 3(d), the slope signs of the two bands are opposite in Figure 3(e), but those are the same in Figure 3(f). Such a phenomenon is also closely related to the variation of the valley Chern numbers between the two SCs. Therefore, by rotating the WMRs, we can realize tunable valley topological transports of sound.

To demonstrate the robustness of these edge states, we design the topological waveguides T1–T3 with the straight and V-shaped domain walls. Figures 4(a)–4(c) show the simulated intensity distributions through T1–T3 at 17.0 kHz. Note that the valley edge states can pass through the V-shaped domain wall with high transmission for three cases, in which the sound transmissions are almost the same as those of the straight domain wall.

Next, we experimentally measure the transmittance spectra of T1–T3 with straight (blue dashed lines) and V-shaped (red solid lines) domain walls. The experimental setup is shown in Figure 5(a), in which the topological waveguide is placed into a planar waveguide composed of two parallel PMMA

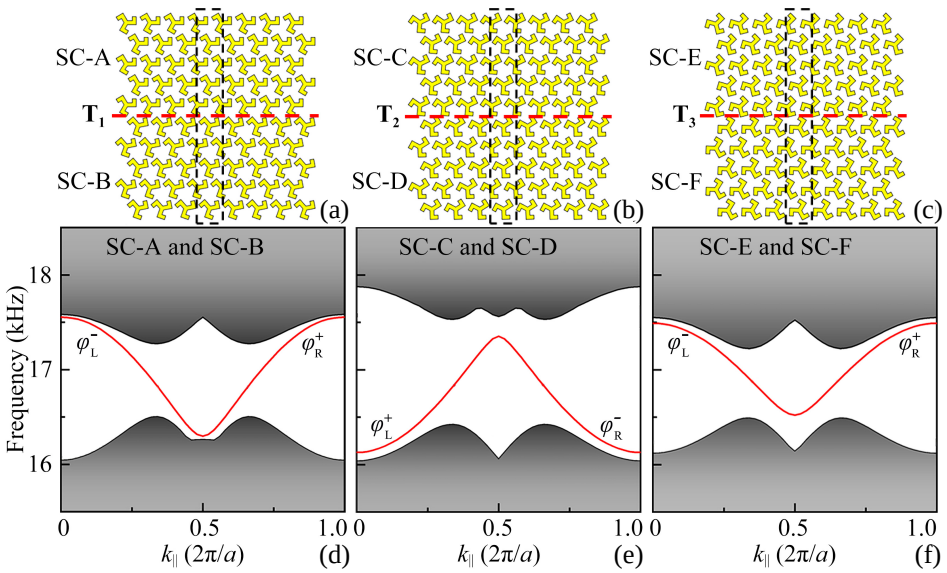

Figure 3. Schematic of the topological waveguides (a) T1, (b) T2, and (c) T3, which are composed of the SC-A and SC-B, the SC-C and SC-D, and the SC-E and SC-F, respectively. Red dashed lines and black dashed rectangles denote the domain walls and supercells, respectively. Dispersion relations of the supercells for (d) T1, (e) T2, and (f) T3.

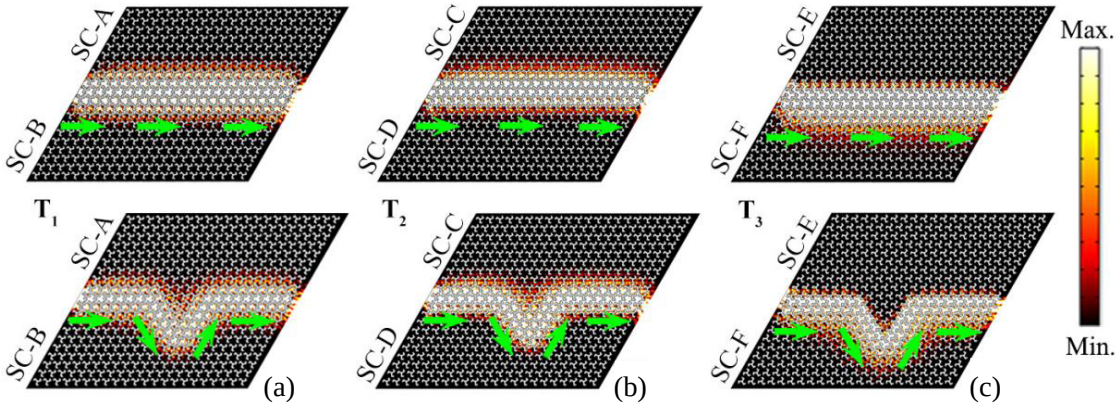

Figure 4. Simulated intensity distributions through the straight and V-shaped domain walls of the topological waveguides (a) T1, (b) T2, and (c) T3 at 17.0 kHz.

plates. The wedge-shaped absorbing foams are placed at the boundaries of the waveguide to realize an anechoic experimental environment. A broadband sound signal is emitted by the loudspeaker driven by a power amplifier and is placed at the left entrance of the domain wall. In the measurement of the transmission spectra, a 1/4 inch microphone (Brüel & Kjær-4961) is used to measure sound signals with and without the sample along the green dashed line which is placed 5 mm away from the right side of the sample, and acoustic pressure amplitudes at each position can be retrieved by using the PULSE Labshop software. Figures 5(b)–5(d) show the transmittance spectra through T1–T3 with the straight and V-shaped domain walls. We find that two types of results agree well with each other for the three cases, further verifying the robustness of the valley edge states experimentally.

Furthermore, we conduct another experiment to demonstrate tunable topological refractions of sound through T1–T3. As shown in Figure 6, the incident sound source is located at the left side of the straight domain wall at 17.0 kHz, and the output sound beams are refracted into air at the zigzag

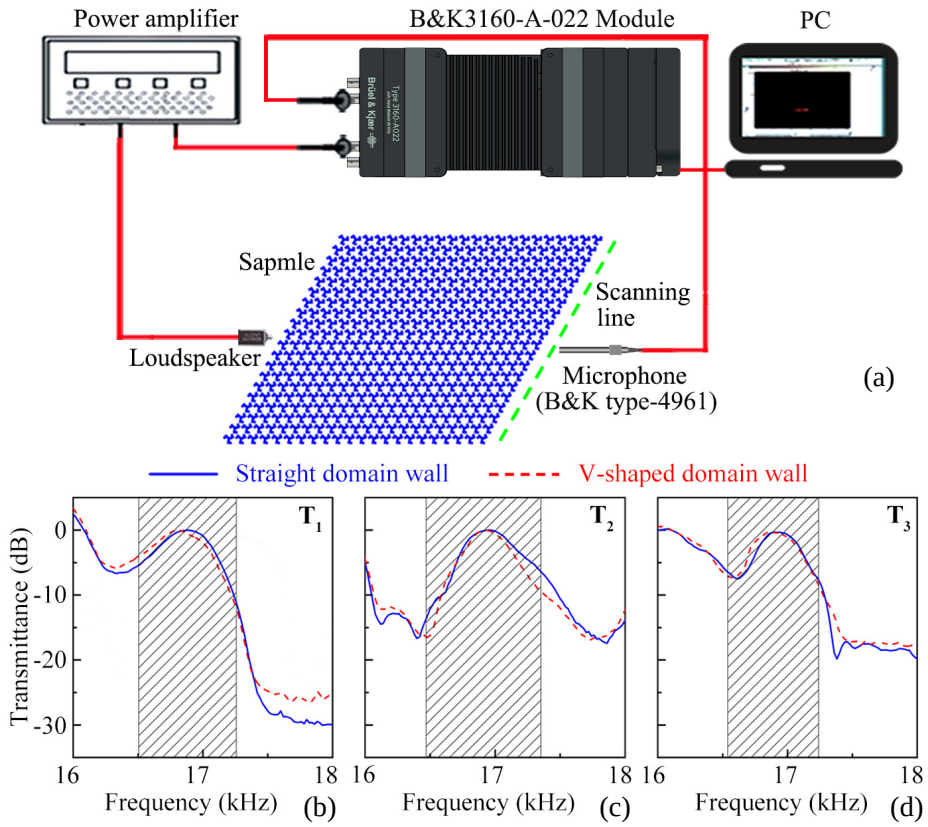

Figure 5. (a) Experimental set-up. Measured transmittance spectra through (b) T1, (c) T2, and (d) T3 with the straight and V-shaped domain walls.

terminal. We can see that the right-moving edge states through T1 and T3 are projected from the valley K, while that through T2 is projected from the valley K′. Due to the larger wave vector in air, three directional out-coupling sound beams can be obtained for the three cases. We observe the coexistence of positive and negative refractions for T1 and T3, and the characteristics of sound refraction are almost the same owing to the projection from the same valley K. However, for T2, three output sound beams negatively refract from the domain wall into the air at the zigzag terminal. The measured and simulated results [shown on the bottom of Figures 6(a)–6(c)] agree well with each other. Therefore, we can realize the tunable topological refractions at the fixed frequency band and terminal by simply rotating the WMRs in the VSCs.

To theoretically explain this, we introduce the Brillouin zone and the equifrequency contour of air (black open regular hexagons and red open circles) which corresponds to the relative values of incident and refracted wavevectors (denoted as $\mathbf{K}$ and $\mathbf{k}$), respectively. By using the phase-matching condition to the terminal interface parallel to $\mathbf{e}_{\text{zig}}$ [11, 30], we theoretically calculate the refraction angles θ_r by $\mathbf{k} \cdot \mathbf{e}_{\text{zig}} = \mathbf{K} \cdot \mathbf{e}_{\text{zig}}$ (See the Supporting Information). The theoretical refraction angles θ_r for T1 and T3 are 33.7°, −17°, and −56.6° (black open arrows), and those for T2 are −3.6°, −42.9°, and −93.7° at 17.0 kHz, which agree well with both measured and simulated results.

Finally, we simulate the topological refractions through T1–T3 with the V-shaped domain wall at 17.0 kHz (See the Supporting Information). It is noted that the characteristics of sound refraction agree well with those for the straight domain wall, further demonstrating the robustness of the topological refractions of valley edge states. Therefore, based on the triple AVH phase transitions, we realize tunable topological refractions in the topological waveguides by simply rotating the WMRs.

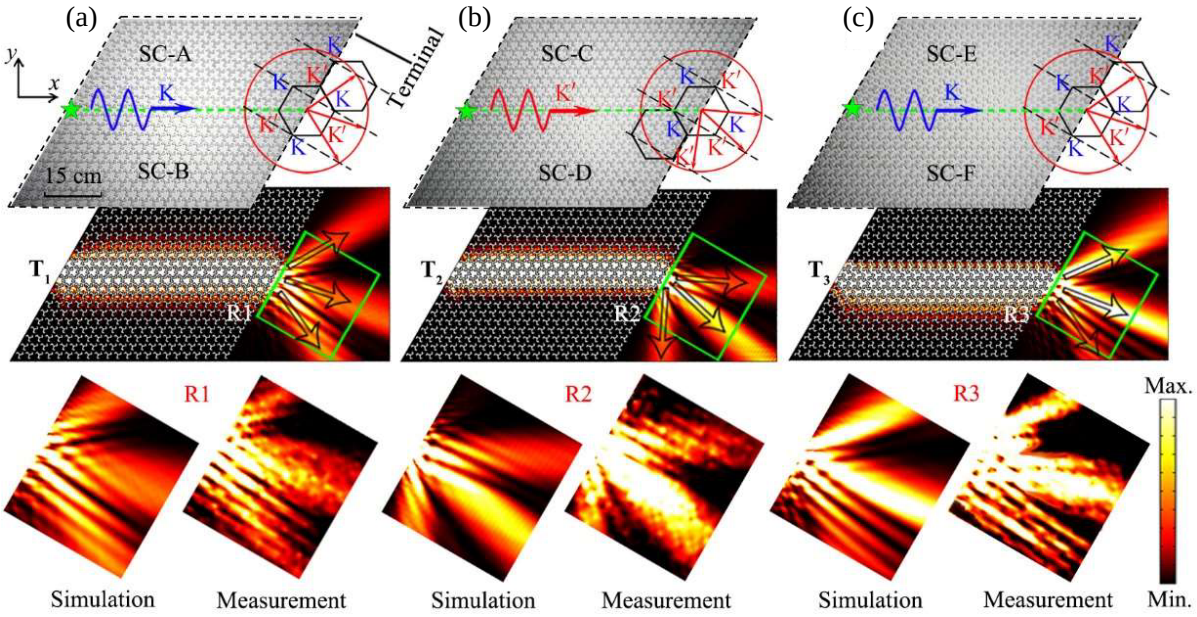

Figure 6. Schematic of the out-coupling of edge states projected from the valley K(K′) passing through the zigzag terminal at 17.0 kHz based on the phase-matching condition for (a) T1, (b) T2 and (c) T3. Black open regular hexagons and red open circles represent the Brillouin zone and the equifrequency curve of air, respectively. Green stars represent point sound sources. Black open arrows refer to the theoretical refraction angles. 6 insets on the bottom are the simulated and measured intensity distributions in green open rectangles R1–R3.

3. CONCLUSIONS

In conclusion, we have experimentally demonstrated tunable topological refractions by VSCs with triple valley Hall phase transitions. By simply rotating the WMRs from 0° to 60°, we realize a triple valley Hall phase transition in the VSCs and design the topological waveguides T1, T2, and T3 composed of two VSCs. Both simulated and experimental results show that the obtained edge states can support valley topological transports and are almost immune to backscattering against sharp bends, showing high robustness of edge states. More interestingly, by simply rotating the WMRs, we can experimentally realize the tunable topological refractions, that is, the coexistence of positive and negative refractions for T1 and T3, and the negative refractions for T2, which are closely related to the valley edge states projected by the valley K and K′. Finally, the robustness of the topological refractions is also discussed in detail. Our work provides a new route for designing valley topological materials with tunable topological refractions, which has great potential in the applications of valley-selective sound emitters and splitters, multi-directional sound antennas, and communication devices.

SUPPORTING INFORMATION

This part provides the description of the Berry curvatures of SC-A and SC-B, the calculation of theoretical refraction angles, and the robustness of topological refraction of sound. The supporting figures can be found at the end of the paper.

ACKNOWLEDGMENT

D. Jia and Y. Wang contributed equally to this work. This work was supported by the National Natural Science Foundation of China (Grant Nos. 11774137, 51779107 and 12174159), the China Postdoctoral

Science Foundation (Grant No. 2020M671351), and the Postdoctoral Research Funding Program of Jiangsu Province (Grant No. 2021K567C).

CONFLICT OF INTEREST

The authors declare no conflict of interest.

REFERENCES

1. Xiao, D., W. Yao, and Q. Niu, "Valley-contrasting physics in graphene: Magnetic moment and topological transport," *Phys. Rev. Lett.*, Vol. 99, No. 23, 236809, 2007, doi: 10.1103/PhysRevLett.99.236809.
2. Zeng, H., J. Dai, W. Yao, D. Xiao, and X. Cui, "Valley polarization in Mos2 monolayers by optical pumping," *Nat. Nanotechnol.*, Vol. 7, No. 8, 490–493, 2012, doi: 10.1038/nnano.2012.95.
3. Zhang, F., A. H. MacDonald, and E. J. Mele, "Valley chern numbers and boundary modes in gapped bilayer graphene," *Proc. Natl. Acad. Sci.*, Vol. 110, No. 26, 10546–10551, USA, 2013, doi: 10.1073/pnas.1308853110.
4. Ju, L., Z. Shi, N. Nair, Y. Lv, C. Jin, J. Velasco, Jr., C. Ojeda-Aristizabal, H. A. Bechtel, M. C. Martin, A. Zettl, J. Analytis, and F. Wang, "Topological valley transport at bilayer graphene domain walls," *Nature*, Vol. 520, No. 7549, 650–655, 2015, doi: 10.1038/nature14364.
5. Schaibley, J. R., H. Yu, G. Clark, P. Rivera, J. S. Ross, K. L. Seyler, W. Yao, and X. Xu, "Valleytronics in 2D materials," *Nat. Rev. Maters*, Vol. 1, No. 11, 16055, 2016, doi: 10.1038/natrevmats.2016.55.
6. Li, J., R. X. Zhang, Z. Yin, J. Zhang, K. Watanabe, T. Taniguchi, C. Liu, and J. Zhu, "A valley valve and electron beam splitter," *Science*, Vol. 362, No. 6419, 1149–1152, 2018, doi: 10.1126/science.aao5989.
7. Ma, T. and G. Shvets, "All-Si valley-Hall photonic topological insulator," *New J. Phys.*, Vol. 18, No. 2, 025012, 2016, doi: 10.1088/1367-2630/18/2/025012.
8. Wu, X., Y. Meng, J. Tian, Y. Huang, H. Xiang, D. Han, and W. Wen, "Direct observation of valley-polarized topological edge states in designer surface plasmon crystals," *Nat. Commun.*, Vol. 8, No. 1, 1304, 2017, doi: 10.1038/s41467-017-01515-2.
9. Dong, J. W., X. D. Chen, H. Zhu, Y. Wang, and X. Zhang, "Valley photonic crystals for control of spin and topology," *Nat. Mater.*, Vol. 16, No. 3, 298–302, 2017, doi: 10.1038/nmat4807.
10. Chen, X. D., F. L. Zhao, M. Chen, and J. W. Dong, "Valley-contrasting physics in all-dielectric photonic crystals: Orbital angular momentum and topological propagation," *Phys. Rev. B*, Vol. 96, No. 2, 020202, 2017, doi: 10.1103/PhysRevB.96.020202.
11. Gao, F., H. R. Xue, Z. J. Yang, K. F. Lai, Y. Yu, X. Lin, Y. D. Chong, G. Shvets, and B. L. Zhang, "Topologically protected refraction of robust kink states in Valley photonic crystals," *Nat. Phys.*, Vol. 14, No. 2, 140–144, 2017, doi: 10.1038/nphys4304.
12. Gao, Z., Z. J. Yang, F. Gao, H. R. Xue, Y. H. Yang, J. W. Dong, and B. L. Zhang, "Valley surface-wave photonic crystal and its bulk edge transport," *Phys. Rev. B*, Vol. 96, No. 20, 201402, 2017, doi: 10.1103/PhysRevB.96.201402.
13. Chen, Q. L., L. Zhang, M. J. He, Z. J. Wang, X. Lin, F. Gao, Y. H. Yang, B. L. Zhang, and H. S. Chen, "Valley-Hall photonic topological insulators with dual-band kink states," *Adv. Opt. Mate.*, Vol. 7, No. 15, 1900036, 2019, doi: 10.1002/adom.201900036.
14. Kang, Y. H., X. Ni, X. J. Cheng, A. B. Khanikaev, and A. Z. Genack, "Pseudo-spin-valley coupled edge states in a photonic topological insulator," *Nat. Commun.*, Vol. 9, No. 1, 1–7, 2018, doi: 10.1038/s41467-018-05408-w.
15. Shalaev, M. I., W. Walasik, A. Tsukernik, Y. Xu, and N. M. Litchinitser, "Robust topologically protected transport in photonic crystals at telecommunication wavelengths," *Nat. Nanotech.*, Vol. 14, No. 1, 31, 2018, doi: 10.1038/s41565-018-0297-6.

16. Noh, J., S. Huang, K. P. Chen, and M. C. Rechtsman, "Observation of photonic topological valley Hall edge states," *Phys. Rev. Lett.*, Vol. 120, No. 6, 063902, 2018, doi: 10.1103/PhysRevLett.120.063902.
17. Yang, Y., H. Jiang, and Z. H. Hang, "Topological valley transport in two-dimensional honeycomb photonic crystals," *Sci. Rep.*, Vol. 8, No. 1, 1588, 2018, doi: 10.1038/s41598-018-20001-3.
18. Yang, Y. H., Z. Gao, H. R. Xue, L. Zhang, M. J. He, Z. J. Yang, R. Singh, Y. D. Chong, B. L. Zhang, and H. S. Chen, "Realization of a three-dimensional photonic topological insulator," *Nature*, Vol. 565, No. 7741, 622–626, 2019, doi: 10.1038/s41586-018-0829-0.
19. Zeng, Y., U. Chattopadhyay, B. Zhu, B. Qiang, J. Li, Y. Jin, L. Li, A. G. Davies, E. H. Linfield, B. Zhang, Y. Chong, and Q. J. Wang, "Electrically pumped topological laser with valley edge modes," *Nature*, Vol. 578, No. 7794, 246–250, 2020, doi: 10.1038/s41586-020-1981-x.
20. Pal, R. K. and M. Ruzzene, "Edge waves in plates with resonators: An elastic analogue of the quantum valley Hall effect," *New J. Phys.*, Vol. 19, No. 2, 025001, 2017, doi: 10.1088/1367-2630/aa56a2.
21. Huo, S. Y., J. J. Chen, H. B. Huang, and G. L. Huang, "Simultaneous multi-band valley-protected topological edge states of shear vertical wave in two-dimensional phononic crystals with veins," *Sci. Rep.*, Vol. 7, No. 1, 10335, 2017, doi: 10.1038/s41598-017-10857-2.
22. Yan, M., J. Y. Lu, F. Li, W. Y. Deng, X. Q. Huang, J. H. Ma, and Z. Y. Liu, "On-chip valley topological materials for elastic wave manipulation," *Nat. Mater.*, Vol. 17, No. 11, 993–998, 2018, doi: 10.1038/s41563-018-0191-5.
23. Wang, J. and J. Mei, "Topological valley-chiral edge states of lamb waves in elastic thin plates," *Appl. Phys. Express*, Vol. 11, No. 5, 057302, 2018, doi: 10.7567/apex.11.057302.
24. Fan, H., B. Xia, L. Tong, S. Zheng, and D. Yu, "Elastic higher-order topological insulator with topologically protected corner states," *Phys. Rev. Lett.*, Vol. 122, No. 20, 204301, 2019, doi: 10.1103/PhysRevLett.122.204301.
25. Yang, L. Y., K. P. Yu, B. Bonello, B. Djafari-Rouhani, W. Wang, and Y. Wu, "Abnormal topological refraction into free medium at subwavelength scale in valley phononic crystal plates," *Phys. Rev. B*, Vol. 103, No. 18, 184303, 2021, doi: 10.1103/PhysRevB.103.184303.
26. Huang, H. B., J. J. Chen, and S. Y. Hou, "Recent advances in topologic alelastic metamaterials," *J. Phys. Condens. Mat.*, Vol. 33, No. 50, 503002, 2021, doi: 10.1088/1361-648X/ac27d8.
27. Ye, L. P., C. Y. Qiu, J. Y. Lu, X. H. Wen, Y. Y. Shen, M. Z. Ke, F. Zhang, and Z. Y. Liu, "Observation of acoustic valley vortex states and valley-chirality locked beam splitting," *Phys. Rev. B*, Vol. 95, No. 17, 174106, 2017, doi: 10.1103/PhysRevB.95.174106.
28. Lu, J. Y., C. Y. Qiu, L. P. Ye, X. Y. Fan, M. Z. Ke, F. Zhang, and Z. Y. Liu, "Observation of topological valley transport of sound in sonic crystals," *Nat. Phys.*, Vol. 13, No. 4, 369–374, 2016, doi: 10.1038/nphys3999.
29. Lu, J. Y., C. Y. Qiu, W. Y. Deng, X. Q. Huang, F. Li, F. Zhang, S. Q. Chen, and Z. Y. Liu, "Valley topological phases in bilayer sonic crystals," *Phys. Rev. Lett.*, Vol. 120, No. 11, 116802, 2018, doi: 10.1103/PhysRevLett.120.116802.
30. Zhang, Z., Y. Tian, Y. H. Wang, S. X. Gao, Y. Cheng, X. J. Liu, and J. Christensen, "Directional acoustic antennas based on valley-Hall topological insulators," *Adv. Mater*, Vol. 30, 1803229, 2018, doi: 10.1002/adma.201803229.
31. Zhang, Z. W., Y. Tian, Y. Cheng, Q. Wei, X. J. Liu, and J. Christensen, "Topological acoustic delay line," *Phys. Rev. Appl.*, Vol. 9, No. 3, 034032, 2018, doi: 10.1103/PhysRevApplied.9.034032.
32. He, C., S. Y. Yu, H. Ge, H. Wang, Y. Tian, H. Zhang, X. C. Sun, Y. B. Chen, J. Zhou, M. H. Lu, and Y. F. Chen, "Three-dimensional topological acoustic crystals with pseudospin-valley coupled saddle surface states," *Nat. Commun.*, Vol. 9, No. 1, 4555, 2018, doi: 10.1038/s41467-018-07030-2.
33. Yang, Y. H., Z. J. Yang, and B. L. Zhang, "Acoustic valley edge states in a graphene-like resonator system," *J. Appl. Phys.*, Vol. 123, No. 9, 091713, 2018, doi: 10.1063/1.5009626.

34. Zhu, Z. X., X. Q. Huang, J. Y. Lu, M. Yan, F. Li, W. Y. Deng, and Z. Y. Liu, "Negative refraction and partition in acoustic valley materials of a square lattice," *Phys. Rev. Appl.*, Vol. 12, No. 2, 024007, 2019, doi: 10.1103/PhysRevApplied.12.024007.
35. Shen, Y. Y., C. Y. Qiu, X. X. Cai, L. P. Ye, J. Y. Lu, M. Z. Ke, and Z. Y. Liu, "Valley-projected edge modes observed in underwater sonic crystals," *Appl. Phys. Lett.*, Vol. 114, No. 2, 023501, 2019, doi: 10.1063/1.5049856.
36. Xie, B. Y., H. Liu, H. Cheng, Z. Y. Liu, S. Q. Chen, and J. G. Tian, "Acoustic topological transport and refraction in a Kekulé lattice," *Phys. Rev. Appl.*, Vol. 11, No. 4, 044086, 2019, doi: 10.1103/physrevapplied.11.044086.
37. Tian, Z., C. Shen, J. Li, E. Reit, H. Bachman, J. E. S. Socolar, S. A. Cummer, and T. J. Huang, "Dispersion tuning and route reconfiguration of acoustic waves in valley topological phononic crystals," *Nat. Commun.*, Vol. 11, No. 1, 762, 2020, doi: 10.1038/s41467-020-14553-0.
38. Wang, M. D., W. Y. Zhou, L. Y. Bi, C. Y. Qiu, M. Z. Ke, and Z. Y. Liu, "Valley-locked waveguide transport in acoustic heterostructures," *Nat. Commun.*, Vol. 11, No. 1, 3000, 2020, doi: 10.1038/s41467-020-16843-z.
39. Jia, D., Y. Ge, H. R. Xue, S. Q. Yuan, H. X. Sun, Y. H. Yang, X. J. Liu, and B. L. Zhang, "Topological refraction in dual-band valley sonic crystals," *Phys. Rev. B*, Vol. 103, No. 14, 144309, 2021, doi: 10.1103/PhysRevB.103.144309.
40. Huang, Z., J. H. Wu, C. Wang, S. K. Yang, and F. Y. Ma, "Resonant-scattering hybrid device for multiband acoustic topology valley transmission," *Phys. Rev. B*, Vol. 104, No. 9, 094110, 2021, doi: 10.1103/PhysRevB.104.094110.
41. Qu, H. F., X. N. Liu, and G. K. Hu, "Topological valley states in sonic crystals with Willis coupling," *Appl. Phys. Lett.*, Vol. 119, No. 5, 051903, 2021, doi: 10.1063/5.0055789.
42. He, H. L., C. Y. Qiu, L. P. Ye, X. X. Cai, X. Y. Fan, M. Z. Ke, F. Zhang, and Z. Y. Liu, "Topological negative refraction of surface acoustic waves in a Weyl phononic crystal," *Nature*, Vol. 560, No. 7716, 61–64, 2018, doi: 10.1038/s41586-018-0367-9.
43. Yang, Y. H., H. X. Sun, J. P. Xia, H. R. Xue, Z. Gao, Y. Ge, D. Jia, Y. D. Chong, and B. L. Zhang, "Topological triply degenerate point with double Fermi arcs," *Nat. Phys.*, Vol. 15, No. 7, 645–649, 2019, doi: 10.1038/s41567-019-0502-z.